Structural information from the Raman spectrum of amorphous silicon

D. Beeman
Department of Physics, Harvey Mudd College, Claremont, California 91711

R. Tsu
Energy Conversion Devices, Inc., 1675 West Maple Road, Troy, Michigan 48084
and Instituto de Fisica e Quimica de Sao Carlos, Universidade de São Paulo, 13.560 Sao Carlos, S.P. Brazil

M. F. Thorpe
Department of Physics and Astronomy, Michigan State University, East Lansing, Michigan 48224
(Received 14 January 1985)

The Raman scattering from various model structures for amorphous silicon is computed. It is shown that the *width* of the "optic peak" increases roughly linearly with the rms bond-angle distortion $\Delta\theta_b$ of the network. The experimentally observed linewidths lead to $7.7° \leq \Delta\theta_b \leq 10.5°$. The smaller linewidths (and hence angles) correspond to networks that have been annealed at higher temperatures. These results are consistent with model-building experience which shows that it is impossible to construct fully bonded amorphous networks with $\Delta\theta_b \leq 6.6°$.

I. INTRODUCTION

Despite nearly fifteen years of extensive study, the precise nature of the microscopic structure of amorphous silicon is still not understood. Diffraction experiments lead to a radial distribution function (RDF) that is consistent with continuous random network models. However, it is very difficult, to almost impossible, to extract quantities like the rms bond angle deviation $\Delta\theta_b$ and the dihedral angle distribution from the measured RDF. Knowledge of such quantities would be useful to give a more detailed description of the network, and also to be able to differentiate between different models. This latter point is of particular interest to us here. In general, we do not expect samples of amorphous silicon grown under different conditions to be identical. Such differences are not easily apparent in the RDF and moreover, the RDF requires considerable data taking and subsequent analysis.

We propose that the one-phonon Raman scattering provides a simple and reliable experimental method to distinguish between samples and further, we show, on the basis of model calculations, that the width of the "optic peak" increases roughly linearly with $\Delta\theta_b$. These ideas have been around in the literature for some time but we quantify them in this paper. We give a definition of $\Delta\theta_b$ that is operationally useful. This is nontrivial as the line shape can be very asymmetric. From our model calculations we find that the linewidth (Γ) in cm^{-1} and $\Delta\theta_b$ in degrees are related by

$$\Gamma = 15 + 6\Delta\theta_b \ . \tag{1}$$

We note that Tsu, Gonzalez-Hernandez, and Pollack[1] have conjectured that

$$\Gamma^2 = (32)^2 + (6.75\Delta\theta_b)^2 \tag{2}$$

using arguments based on the deformation of crystalline silicon. Over the experimentally accessible range $64 \leq \Gamma \leq 82$ cm^{-1} we note that (1) and (2) are essentially indistinguishable.

II. THE MODEL

In order to calculate the Raman spectra, three ingredients are needed: (A) a structural model, (B) a potential to describe the harmonic vibrations of this structure about equilibrium, and (C) an interaction to describe the Raman scattering process.

This route was first taken by Alben *et al.*[2] We have followed it again using a number of different and larger models. We have paid particular attention to the effects of *angular distortions* in the structural models upon the Raman spectra. We comment on these three aspects as follows.

(A) The structural models examined are listed in Table I together with their characteristics. The models are fully relaxed as described by Steinhardt *et al.*[3] The models *GE* 201 (Ref. 3), *GE* 500 (Ref. 4), and *GE* 519 (Ref. 5) were built by Steinhardt *et al.*,[3] Polk and Boudreaux,[4] and Polk,[5] respectively. The *GE* 563 (Ref. 6) model was originally built by Evans for SiO_2 but has had the oxygen atoms removed. It is relaxed to Si bond angles and bond length, but the SiO_2 topology is retained. The *H* 1 model was built by Connell and Temkin[7] and contains no odd-membered rings. The other *H* models are reconstructed from the *H* 1 model by Beeman and Bobbs[8] and contain successively more odd-membered rings and larger angular distortions. We refer the interested reader to Ref. 8 for more information on the reconstruction process.

We thus have a set of fully relaxed networks that have various angular distortions. These differing angular distortions reflect different topologies. All the models have "free" boundaries and have been fully relaxed using the Keating potential.[9] They all have rms bond length deriva-

TABLE I. Relevant parameters for the models studied where $\Delta r/r_0$ is the rms fractional width of the bond lengths about the mean length r_0 and $\Delta\theta_b$ is the rms angular width in degrees about the tetrahedral angle. The widths $\Delta\omega_1$ (for mechanism 1) and $\Delta\omega_2$ (for mechanism 2) were obtained from Fig. 1 as described in the text.

Model	$\Delta r/r_0$	$\Delta\theta_b$ (deg)	$\Delta\omega_1$ (cm^{-1})	$\Delta\omega_2$ (cm^{-1})
GE 201	0.009	6.6		
GE 500	0.023	6.7	32	56
GE 519	0.011	7.3	37	61
GE 563	0.026	11.0	52	85
H 1	0.014	9.1	50	76
H 2	0.015	10.2		
H 4	0.016	10.9		
H 5	0.017	11.6	60	88
H 6	0.017	13.4		

tions Δr that are $\lesssim 2\%$ of the mean bond length r_0. The rms angular distortions $\Delta\theta_b$ range from 6.6° up to 13.4°. This gives a good range of $\Delta\theta_b$ and allows us to study the effect of structural distortion on the Raman spectra.

We note that, while the RDF does show small differences for different models,[8] they are relatively modest. We will show that the Raman spectrum is much more sensitive to structural changes. If a single parameter is to be used to characterize these structural differences we suggest that $\Delta\theta_b$ is the appropriate one. Other parameters, like the distribution of dihedral angles appear to have a less pronounced effect on the Raman scattering.

Crystalline silicon in the diamond cubic structure has $\Delta\theta_b = 0°$. Experience shows that it is not possible to construct homogeneous models with $0° < \Delta\theta_b \lesssim 6.6°$. This is not surprising as there is a discontinuous change in topology in going from a crystalline to an amorphous material. There is therefore a region in $\Delta\theta_b$ parameter space that is not accessible and cannot be explored.

(B) We have chosen a Born potential to describe small vibrations of the network away from equilibrium.[10] Very similar results would have been obtained using a Keating potential and it would have been more consistent to do so as this potential was used to relax the networks. We originally used the Born potential as it is simpler for making analytic calculations of moments, etc. However, we later decided on the more straightforward approach of comparing our numerical results directly with experiment. The Born potential is given by

$$V=\tfrac{1}{2}(\alpha-\beta)\sum_{\langle l,\Delta\rangle}[(\mathbf{u}_l-\mathbf{u}_{l+\Delta})\cdot\mathbf{r}_\Delta(l)]^2 + \frac{\beta}{2}\sum_{\langle l,\Delta\rangle}(\mathbf{u}_l-\mathbf{u}_{l+\Delta})^2 , \tag{3}$$

where $\beta/\alpha=\frac{2}{11}$ and α is chosen so that the maximum frequency $\omega_{\max}=[\frac{8}{3}(\alpha+\beta)/M]^{1/2}$ is at 520 cm^{-1} where M is the silicon mass. This corresponds to the Raman active mode in crystalline silicon. The sum over l goes over the Si atoms and Δ goes over the nearest neighbors. The $r_\Delta(l)$ are unit vectors that join the atom at l to its neighbors at Δ.

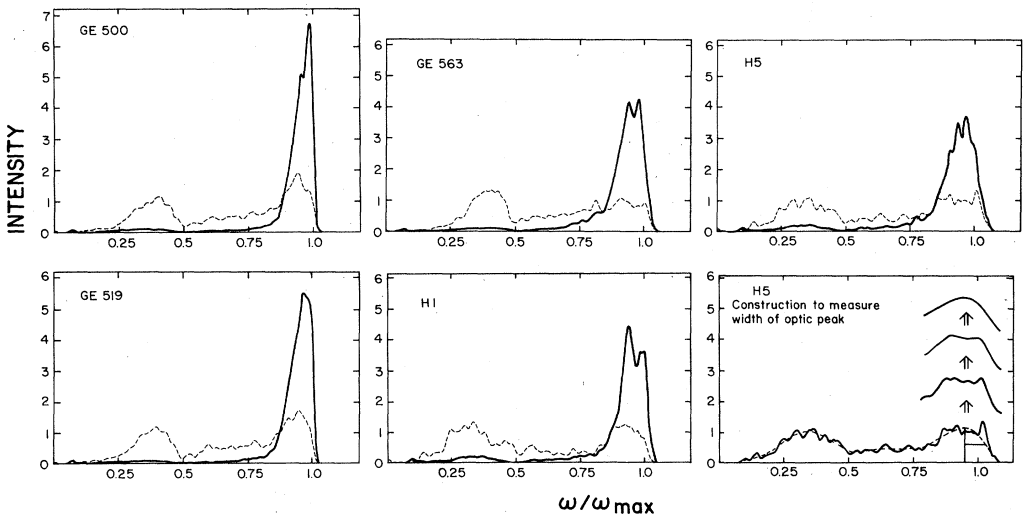

FIG. 1. Raman scattering for five models; the solid and dashed curves are for mechanisms 1 and 2, respectively, and are averaged over all polarization directions. The intensity for the Raman scattering is in arbitrary units and the area under all the curves is normalized to be the same. The last panel illustrates how the width Γ is obtained from the asymmetric "optic peak" as explained in the text. In this case, the solid curve represents mechanism 2, and the dashed curve is the smoothed data.

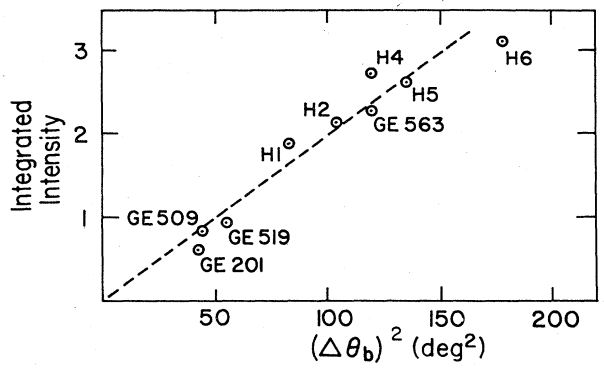

FIG. 2. Total scattered intensity per atom, integrated over all frequencies for the various models studied for mechanism 2, plotted as a function of the mean squared bond angle deviation. The integrated intensity per atom is in arbitrary units and $\Delta\theta_b$ is in degrees. The dashed line is a guide for the eye only.

(C) The most uncertain part of this procedure is to write down the interaction between the radiation field and the phonons that leads to one photon being absorbed from the incident radiation field and another being added to the scattered field at a shifted frequency. The simplest approach is to write down local bond polarizabilities.[2] It is assumed that bonds behave independently, are identical, and have cylindrical symmetry. This gives three independent forms for the polarizability[2]

$$\alpha_1 = A \sum_{\langle l,\Delta\rangle} [\mathbf{r}_\Delta(l)\cdot\mathbf{r}_\Delta(l) - \tfrac{1}{3}I]\mathbf{u}_l\cdot\mathbf{r}_\Delta(l) ,$$

$$\alpha_2 = B \sum_{\langle l,\Delta\rangle} \{\tfrac{1}{2}[\mathbf{r}_\Delta(l)\cdot\mathbf{u}_l + \mathbf{u}_l\cdot\mathbf{r}_\Delta(l)] - \tfrac{1}{3}\mathbf{u}_l\cdot\mathbf{r}_\Delta(l)\} , \quad (4)$$

$$\alpha_3 = C \sum_{\langle l,\Delta\rangle} I\mathbf{u}_l\cdot\mathbf{r}_\Delta(l) .$$

We shall refer to α_1 as mechanism 1, α_2 as mechanism 2, and α_3 as mechanism 3. The parameters A, B, and C are arbitrary constants. For a *perfect* tetrahedral arrangement of the Si atoms as in a diamond cubic crystal

$$\sum_{\Delta} \mathbf{r}_\Delta(l) = 0 \quad (5)$$

so that $\alpha_2 = \alpha_3 = 0$ and all the scattering is produced by mechanism 1 which is therefore responsible for the 520-cm^{-1} line in crystalline silicon. Because of the way the three mechanisms are written, mechanisms 1 and 2 lead to a depolarization ratio of $\rho = \frac{3}{4}$ and mechanism 3 leads to

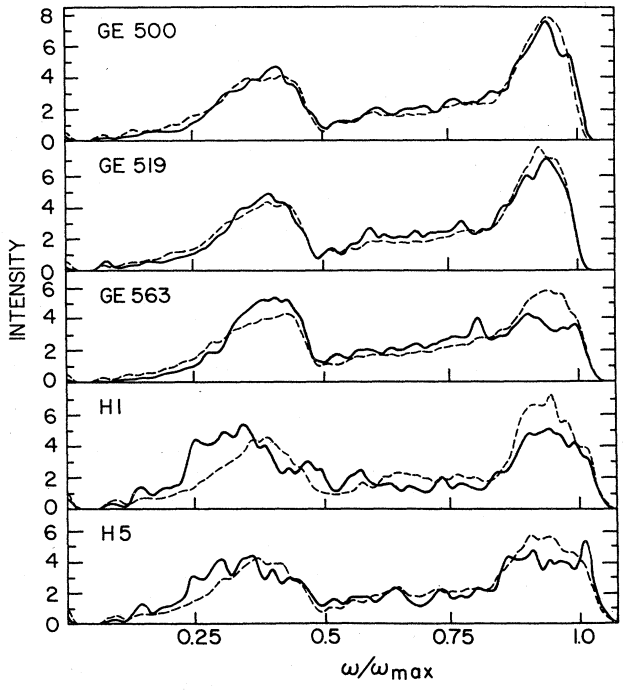

FIG. 3. Raman scattering for mechanism 2 compared to the density of states, averaged over the same interior, fully bonded, atoms. The solid curves are for mechanism 2 (from Fig. 1) and the dashed curves are the density of states. The vertical scale is arbitrary and the areas under all the curves are normalized to be the same.

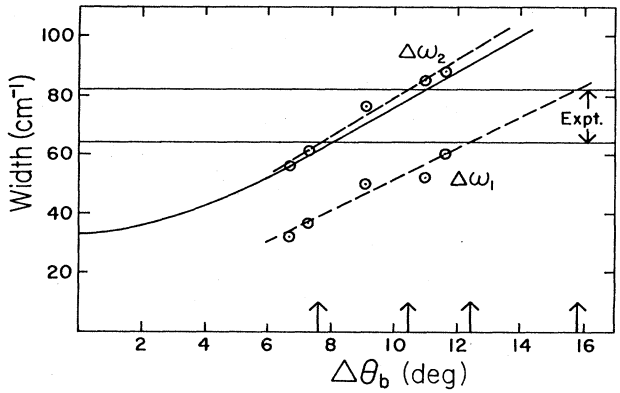

FIG. 4. Widths $\Delta\omega_1$ and $\Delta\omega_2$ from Table I, plotted against $\Delta\theta_b$ in degrees. The curved line is given by Eq. (2) and the two straight lines are drawn by eye to go through the points. The straight line through the $\Delta\omega_2$ points is given in Eq. (1) where $\Gamma = \Delta\omega_2$.

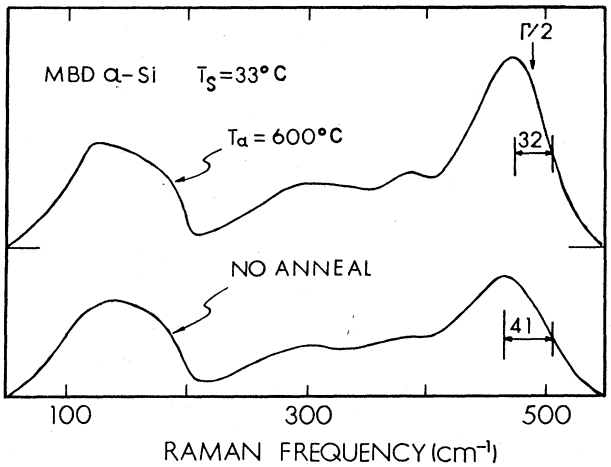

FIG. 5. Two typical Raman spectra $I(\omega)$ for molecular beam deposited (MBD) a-Si at substrate temperature $T_s = 33\,^\circ$C. The top one has been annealed at 600 °C. The upper one has $\Gamma = 64$ cm^{-1} and the lower one has $\Gamma = 82$ cm^{-1}.

$\rho=0$; all independent of the frequency.

We have used the equation of motion technique[11] to compute the Raman scattering per atom from the various structural models for both mechanism 1 and mechanism 2. The results are shown in Fig. 1 for five of the models using both mechanisms, where an average has been taken over the diagonal and off-diagonal elements in the Raman tensor. This is appropriate to the usual experimental setup where unpolarized light is used.

It can be seen that mechanism 1 leads to significant scattering only for $\omega/\omega_{\max}\gtrsim 0.8$ whereas mechanism 2 leads to scattering at all frequencies. The Raman scattering is computed by summing the polarizabilities (4) over only the interior atoms of the network that are fully bonded. Because this number is only ~ 300, there is considerable noise in the computed spectra. This we would expect to disappear, if computations could have been done with larger samples. The computed curves all have a width, shown in the first panel, because the time integration is truncated in the equation of motion method.

In order to extract a width for the "optic peak," the response is smoothed by first discretizing the curves and then averaging over all triples of points as shown in the last panel of Fig. 1. By repeating this process about three times as shown, a smooth curve is obtained which is superimposed onto the original curve as a dashed line. The parameter Γ is defined as twice the half-width on *the high-frequency side* at half the maximum height. This seems, to us, the best working definition as the scattering cuts off abruptly on the high-frequency side but not on the low-frequency side. Other definitions of the width can lead to almost any width when the line becomes less distinct as for mechanism 2 and the $H5$ structure. When the line is well-defined as for mechanism 1 and the $GE519$ structure, there is no problem. We use this same definition of the Γ in obtaining a width from the experimental results.

Values of the widths are shown in Table I, where $\omega_{\max}$ was taken as 510 cm^{-1} which gives a slightly better fit, due to a slight increase in bond length.[12] The corresponding $\omega_{\max}$ for c-Si is 520 cm^{-1}.

The total integrated intensity for mechanism 1 is constant. The increasing angular disorder $\Delta\theta_b$ merely spreads the intensity over a wider range. On the other hand, the integrated intensity from mechanism 2 increases roughly linearly with $(\Delta\theta_b)^2$ as shown in Fig. 2. In Fig. 3, we show that mechanism 2 leads to a spectrum that is very similar to the density of states. This agrees with the postulated result of Shuker and Gammon[13] although we do not find their reasoning convincing.

In Fig. 4 we show the widths $\Delta\omega_1$ and $\Delta\omega_2$ obtained for mechanisms 1 and 2 plotted against $\Delta\theta_b$. It can be seen that they are both increasing roughly linearly with $\Delta\theta_b$ in the accessible range but that $\Delta\omega_2$ is considerably larger than $\Delta\omega_1$.

Although all three mechanisms contribute to the Raman spectrum of amorphous silicon and give an optic peak width increasing linearly with $\Delta\theta_b$, we feel that mechanism 2 best characterizes the effect of distortion on the spectra. Mechanisms 1 and 2 contribute to both polarized and depolarized scattering, whereas mechanism 3 contributes only to polarized scattering. The total integrated Raman scattering from amorphous silicon is about 8 times as intense as in crystalline silicon when the appropriate absorption corrections are made. Thus, mechanism 1 would have roughly $\frac{1}{7}$ of the integrated intensity of the others and thus makes a lesser contribution to the overall spectrum, although it makes a significant contribution to the optic peak height. Another reason for preferring mechanism 2 is that the experimentally observed values of Γ are from 64 to 82 cm^{-1}. If we use mechanism 1, this leads to rather large distortions in the range $12.5°<\Delta\theta_b<15.7°$ as shown by the arrows in Fig. 4. However, mechanism 2 leads to the more reasonable range of $7.7°<\Delta\theta_b<11°$.

In all the computation in this work, we refer to the reduced Raman intensity $R(\omega)$ with the thermal and harmonic oscillator factors removed so that the observed intensity $I(\omega)$ is

$$I(\omega)=\frac{n(\omega)+1}{\omega}R(\omega)\ . \tag{6}$$

In Fig. 5, we have shown examples of the two extreme experimental results for the Raman intensity $I(\omega)$. In both cases, there is no crystallization as evidenced by the lack of a sharp spike at 520 cm^{-1}. The annealed sample has $\Gamma=64$ cm^{-1} whereas the unannealed sample has $\Gamma=82$ cm^{-1}.

III. CONCLUSION

In this paper, we have quantified previous suggestions[14] that the width of the "optic peak" in the Raman scattering can be a useful indicator of the distortions in the network. In particular, we have given an empirically useful definition of the width and for the first time, have related this width to the angular distortions $\Delta\theta_b$ via Eq. (1). This was done with the help of computations using models, as no reliable independent measure of $\Delta\theta_b$ is currently available experimentally. Such an experiment would, of course, be very valuable. We believe that Eq. (1) provides an easy experimental method of characterizing amorphous silicon.

ACKNOWLEDGMENTS

We would like to thank J. Joannopoulos and A. McGurn for useful discussions. This work was partially funded by ONR under Contract No. N00014-80-C-0610.

[1]R. Tsu, J. Gonzalez-Hernandez, and F. H. Pollack, J. Non-Cryst. Solids **66**, 109 (1984).

[2]R. Alben, D. Weaire, J. E. Smith, Jr., and M. H. Brodsky, Phys. Rev. B **11**, 2271 (1975).

[3]P. Steinhardt, R. Alben, and D. Weaire, J. Non-Cryst. Solids **15**, 199 (1974).

[4]D. E. Polk and D. S. Boudreaux, Phys. Rev. Lett. **31**, 42 (1973).

[5]D. E. Polk, J. Non-Cryst. Solids **5**, 365 (1971).
[6]D. L. Evans, M. P. Teter, and N. F. Borrelli, J. Non-Cryst. Solids **17**, 245 (1975).
[7]G. A. N. Connell and R. J. Temkin, Phys. Rev. B **9**, 5323 (1974).
[8]D. Beeman and B. Bobbs, Phys. Rev. B **12**, 1399 (1975).
[9]P. N. Keating, Phys. Rev. **145**, 637 (1966).
[10]See, for example, M. F. Thorpe, in *Vibrational Spectroscopy of Molecular Liquids and Solids,* Vol. B56 of NATO, Advanced Studies Institute Series, edited by S. Bratos and R. M. Pick (Plenum, New York 1980), p. 341.
[11]D. Beeman and R. Alben, Adv. Phys. **26**, 339 (1977).
[12]P. Steinhardt, R. Alben, and D. Weaire, J. Non-Cryst. Solids **15**, 199 (1974).
[13]R. Shuker and R. W. Gammon, Phys. Rev. Lett. **25**, 222 (1970).
[14]See, for example, J. Lannin, in *Amorphous Hydrogenated Silicon,* edited by J. Pankove (Academic, New York, 1984), Vol. II.